Indonesian Geotechnical Journal, December 2024, Vol 3 (3). Page 17-30
DOI: https://doi.org/10.56144/igj.v3i3.104
EISSN: 2829-7520
https://indonesian-geotechnical-journal.org/index.php/JGI/issue/archive

Evolution of Crushing Surface of Ta-d Pumice in Triaxial Compression Tests

Itsuki Sato[1,*], Reiko Kuwano[2], Masahide Otsubo[3], Atsushi Mohri[4]
[1] Port and Airport Research Insitute, Yokosuka, Japan, 239-0826; itsukisato1007@gmail.com
[2] Institute of Industrial Science, The University of Tokyo, Tokyo, Japan, 153-8505; kuwano@iis.u-tokyo.ac.jp
[3] Port and Airport Research Insitute, Yokosuka, Japan, 239-0826; otsubo-m@p.mpat.go.jp
[4] Port and Airport Research Insitute, Yokosuka, Japan, 239-0826; mouri-a-p@p.mpat.go.jp
*Correspondence: itsukisato1007@gmail.com

SUBMITTED 25 November 2024 **REVISED** 12 Dec 2024 **ACCEPTED** 23 December 2024

ABSTRACT Crushable porous granular materials like volcanic pumice, distributed worldwide, cause various engineering problems, including slope hazards. These materials are often classified as problematic soils due to their complex mechanical properties, which arise from high compressibility and changes in grain size due to particle crushing. Consequently, their behaviour is typically discussed on a case-by-case basis, and a systematic understanding has yet to be established. This study aims to elucidate the relationship between the mechanical properties and particle crushing of porous granular materials through a series of tests on natural volcanic pumice. The intra-particle void ratio was measured alongside isotropic consolidation and CD/CU triaxial compression tests, with particle crushing assessed before and after the experiments. The results indicate that the intra-particle void ratio correlates with particle size, with larger particles generally having higher porosity. Additionally, the mechanical behaviour of these materials shows high compressibility, and their stress paths resemble those obtained from undrained triaxial tests on loose sand, ultimately reaching the critical state. The relationship between the amount of particle crushing and mean effective stress at the end of the tests can be represented by a single curve for isotropic consolidation tests, CD, and CU triaxial tests, respectively. The amount of crushing generally increases with the progression of axial strain during the compression process, and in CU tests, when reaching the critical state, no further increase in crushing occurs with increased axial strain. Furthermore, critical state and isotropic consolidation state of each material can be represented on its own unique surface, each referred to as a "Crushing Surface," defined by the crushing volume, void ratio, and mean effective stress for that specific soil.

KEYWORDS particle crushing; pumice, porous particle, critical state

1 INTRODUCTION

Crushable soils with high void structures are distributed worldwide and cause a variety of engineering problems. Table 1 shows representative long-distance flow disasters caused by earthquakes in Japan in recent years. It is quite important to study the mechanical behaviour of crushable porous granular material, which is responsible for many of these disasters. Studies relating mechanical properties to slope flow of loose sand have been carried out for many years. Castro (1969) conducted tests on loose sand and showed that loose sand eventually reaches steady state, which he used to distinguish dilatancy properties on the $e - \log p'$ plane. Ishihara et al. (1975) showed that in triaxial tests of loose sand, a point (phase transformation) appears at which the effective mean stress reaches minimum value and the dilatancy behaviour changes from shrinkage to expansion. The steady state of sand has also been organised in some papers as an extension of the critical state theory for clay and is also referred to as critical state (Sasitharan et al., 1994). The difference in void ratio from the critical state line (=steady state line) to the current state at the current effective mean stress is called state parameter (Been and Jefferies, 1985) and is often used in modelling granular materials due to its simplicity of calculation.

There are a number of previous studies on sand crushing. Crushable soils, when sheared, have been found to follow the same undrained stress path as less crushable loose sand (Hyodo et al., 1998), and as the grain size range increases due to crushing, the soil particles are able to pack more efficiently and the position of the critical state on the $e - \log p'$ plane also has a significant impact (Bandini and Coop, 2011). It is known that in one-dimensional compression tests, a large amount of crushing occurs in poorly graded soils leading to efficient packing and the formation of a peculiar normal compression line, whereas the amount of crushing is significantly reduced in soils of well-graded initial gradation and very little crushing is measured in very good graded samples (Altuhafi and Coop, 2011).

Table 1. Representative long-distance flow disasters caused by earthquakes in Japan in recent years summarized in Sato et al. (2024) (Sugimoto et al., 2013; Chiaro et al., 2022; Hashimoto et al., 2023).

Year	Earthquake	Representative areas of slope disaster	Characteristics of slope disaster	Trigger layer
2008	Iwate–Miyagi Nairiku earthquake	Dozou-sawa	Long distance flow	Pumice
2011	Great East Japan earthquake	Shirakawa	Gentle slope, long-distance flow	Pumice, Scoria
2016	Kumamoto earthquakes	Minami Aso	Gentle slope, long-distance flow	Pumice
2018	Hokkaido Eastern Iburi earthquake	Atsuma	Gentle slope, long-distance flow	Pumice

There has also been plenty of research on porous pumice. Soils with internal voids in the particles, such as volcanic granular soils, also undergo significant changes in particle array structure with crushing due to their compressibility, and particle crushing occurs even at relatively low stress levels compared to non-porous materials, so particle crushing has a significant effect on compressive and shear properties at stress levels in the normal engineering range (Sato et al., 2024). Ishikawa and Miura (2011) proposed a void structure model that organises soil voids with porous soil particles in two parts: inter-particle void ratio e_{inter} and intra-particle void ratio e_{intra}. Several attempts have also been made to apply the theory of critical states with state parameters to porous pumice, and Cristofaro et al. (2022) have shown the possibility of explaining the undrained mechanism of pore pressure increase for volcanic soils with the state parameter ψ obtained from static tests.

Due to the wide variation in pumice properties from place to place and the heterogeneity of pumice samples collected from nature, there has been little systematic investigation of the relationship between the mechanical properties and the crushing amount of crushable porous granular material. It is important to investigate the relationship between crushing and mechanical properties in order to understand the mechanical behaviour of crushable porous soils by applying the theory of critical states, because a large increase in crushing amount changes the void ratio for the efficient soil particle structure, changes the position of the critical state on the compression plane, and changes the criterion in the definition of state parameter ψ. If the position of the critical state line for the post-crushing grain size distribution can be formalized, it may become possible to establish a constitutive model for crushable porous granular materials by extending existing models, such as the Severn-Trent sand model (Gajo and Muir Wood, 1999), that describe typical sand responses using state parameters. Establishing such a constitutive model would enable accurate FEM-based analysis of deformation in crushable porous granular materials, such as pumice, potentially having a significant engineering impact in regions where these materials are distributed. However, studies on changes in the critical state line of pumice are limited, and the relationship between pumice crushing and the position of the critical state line remains poorly understood. In this study, isotropic consolidation tests and CD/CU triaxial compression tests were conducted using natural pumice, while measuring the amount of crushing before and after the tests to investigate the effect of crushing on the position of the critical state line.

2 MATERIALS AND PHYSICAL PROPERTIES

2.1 Ta-d pumice

In this study, triaxial test results are discussed for Ta-d pumice, a natural pumice. Ta-d pumice is considered to be one of the layers responsible for the slope hazards in the numerous long-distance flow failures that occurred during the September 2018 Hokkaido Eastern Iburi Earthquake (Zhang et al., 2019; Kawamura et al., 2019; Li et al., 2020; Ishikawa et al., 2021; Sato et al., 2024). The authors and their team conducted a field survey on 12 October 2018 and conducted triaxial tests on the collected Ta-d pumice samples. The collection sites, depositional conditions, basic test results and discussion of the stability of the slope hazards are described in the earlier paper (Sato et al., 2024) and are therefore omitted here. Ta-d pumice is a porous granular material with weak single particles, high water retention and high water content, which can be easily crushed by hand into a liquid state. It is considered to be a suitable example of a natural crushable porous granular material for comparison with artificial pumice.

2.2 Physical properties of the materials

Table 2 shows the physical properties of the experimental material. Soil particle density was measured after sufficient boiling of the milled samples and are the densities of true soil particles, which as far as possible do not include the effects of intra-particle voids. The soil particle density of Ta-d pumice is 2.57 g/cm³, indicating that it has a typical soil particle density. In triaxial tests, only grain sizes between 2 mm and 4.75 mm were extracted by sieving and used.

Table 2. Physical properties of the tested pumice

	ρ_s [g/cm^3]	Particle size (mass ratio)	D_{50} [mm]	Consistency characteristics		
				Liquid limit [%]	Plastic limit [%]	Plasticity index
Ta-d pumice	2.57	2−4.75mm (100%)	3.38	103*	77.9*	24.6*

* Conducted on samples passing a 425 μm sieve in accordance with JIS A 1205.

As mentioned earlier, the void ratio of porous particles can be divided into inter-particle void ratio e_{inter} and intra-particle voids ratio e_{intra}. The respective equations are as follows:

$$e_{intra} = \frac{V_{v\_intra}}{V_s},\ e_{inter} = \frac{V_{v\_inter}}{V_s} \quad (1)$$

where V_{intra} is the volume of the intra-particle voids, V_{inter} is the volume of the inter-particle voids and V_s is the volume of the pure soil particle part without V_{intra}. Although there are several studies on the measurement of intra-particle void ratios for porous granular materials (e.g., Wesley, 2001), a standardized method has yet to be established, and the accuracy of each measurement method remains unclear. In this study, to determine the intra-particle void structure e_{intra} of porous artificial pumice and Ta-d pumice, the intra-particle voids were analysed by paraffin-coated methods and sieve-count methods. These methods were adopted in this study because they are simple, involve minimal variation due to the experimenter, and are considered highly reproducible. Figure 1 shows the intra-particle void ratio of Ta-d pumice. For particles larger than 4.75 mm, the completely dried soil specimens were immersed in a hot paraffin solution so that it forms a film on the surface, which prevents water from entering the soil particles. The water displacement method was then used to determine the density of one whole porous particle, including the air in the intra-particle voids, and e_{intra} was calculated from this, the soil particle density and the dry weight of the particles. Each point plotted by the paraffin coated method is the average of five particles.

For particles smaller than 4.75 mm, it was difficult to apply a thin layer of paraffin solution, making it difficult to test with paraffin-coated methods, so a sieve was used to weigh 400-1100 particles per soil gradation range, from which the intra-particle voids were calculated assuming that the particles

were perfect spheres. This method is tentatively referred to as "sieve-count method" in this paper. For example, for a dry sample of 1.4 mm to 2 mm obtained by sieving, 500 particles were counted and weighed, divided by 500 to obtain the average weight of one particle ($M_{1particle}$), and then, assuming that all particles were perfect spheres with a diameter of 1.7 mm, the volume of one particle ($V_{1particle}$) was calculated to estimate the intra-particle void (e_{intra}) at 1.7 mm diameter as follows:

$$e_{intra} = \frac{V_{intra}}{V_s} = \frac{V_{1particle} - V_s}{V_s} = \frac{V_{1particle} - M_{1particle}/\rho_s}{M_{1particle}/\rho_s} \quad (2)$$

Note that 400-1100 particles were measured together in order to obtain an average of a sufficient number and because the weight of one particle is too light to be measured with a standard high-precision electronic balance. The intra-particle void ratios obtained by this sieve-count method are also plotted in Figure 1. Each data point represents an average of 400-1100 particles per point.

In Figure 1, a linear approximation of $e_{intra} = 0.174 \times \text{Diameter} + 1.750$ was obtained from all but one of the six points with the smallest diameter. There is a tendency for the intra-particle void ratio to decrease as the diameter of the particles decreases, which seems reasonable considering that the smaller the particles are, the less likely they are to have large voids within the particles. There is a distribution in the size of the intra-particle voids. As the particle diameter approaches zero, the number of feasible intra-particles also decreases. It can be assumed that the plot of intra-particle void ratio versus diameter in Figure 1 shows a bending point somewhere in the region of small particle diameters, as indicated by the dotted line, suggesting that the intra-particle void volume approaches zero. In fact, the plot of Ta-d pumice with a diameter of 0.6375 shows a sharp decrease in the intra-particle void. Therefore, it is not originally appropriate to make a linear approximation, but a linear approximate straight line is described to show numerically the trend in intra-particle void properties. If further research is carried out and more plots of intra-particle void ratios in the region of smaller particles are available, a curvilinear approximation should be attempted.

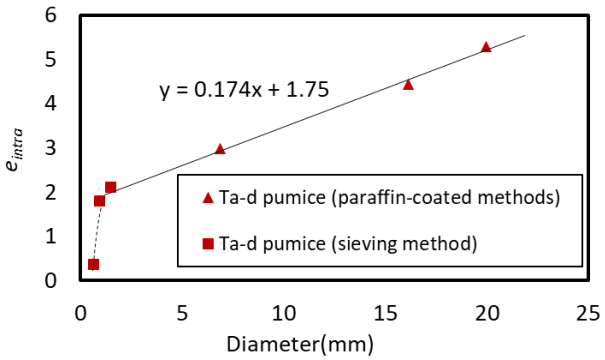

Figure 1. Intra-particle void ratio of Ta-d pumice.

3 TEST PROCEDURE

3.1 Triaxial test

The triaxial tests in this study are broadly divided into two series: the standard triaxial series (ST series) and the crushing evolution series (CE series). The ST series comprised conventional triaxial tests. Conversely, the CE series focused on observing the evolution of crushing during the compression process, with tests performed at varying axial strains at the end of the test.

Table 3 lists all the tests of the standard triaxial series (ST series). The Test ID indicates the test type and initial confining stress. In the Test ID, 'C' denotes the isotropic consolidation test (no compression process), and 'CD/CU' represents the CD/CU triaxial compression test following isotropic consolidation. All tests in the ST series were conducted under saturated conditions, with a

pressure increase rate of 2.5 kPa/min during the consolidation process and an axial strain rate of 1%/min during the triaxial compression process.

Table 4 enumerates the tests for the crushing evolution series (CE series). In the Test ID, the numbers following the underscore signify the axial strain at the end of the test, and 'CD/CU' refers to the CD/CU triaxial compression test after isotropic consolidation. All tests in the CE series were performed under saturated conditions, with an axial strain rate of 1%/min during the triaxial compression process. In the CE series, rapid isotropic consolidation was facilitated by increasing the confining pressure to 200 kPa under undrained conditions before opening the drainage valve for rapid consolidation.

In all tests, only grain sizes between 2 mm and 4.75 mm were used, and the preconsolidation pressure was set at 10 or 20 kPa. The preconsolidation pressure refers to the initial pressure applied to secure and stabilize the specimen, under which the initial specimen dimensions were measured. To minimize crushing during the specimen setting process, particles were gradually added from above using a spoon. Simultaneously, the metal mould (50 mm diameter, 100 mm height) was struck with a hammer and vibrated to achieve the densest packing possible.

Table 3. Test list of standard triaxial series (ST series)

Test ID	Axial strain at the end of the test	Initial void ratio	Initial intra void ratio	Drainage condition		Confining Pressure (kPa)
				Consolidation	Compression	
C30	-	6.95	2.33	Drained	-	30
C100		7.33		Drained	-	100
C200		6.55		Drained	-	200
C400		4.44		Drained	-	400
CD30	15% – 20%	6.34		Drained	Drained	30
CD100		6.74		Drained	Drained	100
CD200		5.93		Drained	Drained	200
CU30		6.59		Drained	Undrained	30
CU100		6.6		Drained	Undrained	100
CU200		5.74		Drained	Undrained	200

Table 4. Test list of crushing evolution series (CE series)

Test ID	Axial strain at the end of the test	Initial void ratio	Initial intra void ratio	Drainage condition		Confining Pressure (kPa)
				Consolidation	Compression	
CD200_2%	2%	6.74	2.33	Drained	Drained	200
CD200_5%	5%	5.99		Drained	Drained	
CD200_10%	10%	6.41		Drained	Drained	
CD200_20%	20%	4.94		Drained	Drained	
CU200_2%	2%	6.42		Drained	Undrained	
CU200_5%	5%	5.78		Drained	Undrained	
CU200_10%	10%	5.66		Drained	Undrained	
CU200_20%	20%	5.32		Drained	Undrained	

Note: Rapid consolidation was carried out for crushing evolution series (CE series).

3.2 Method of quantifying the amount of particle crushing

Various methods have been proposed by researchers from all over the world for indices to quantify crushing. Xiao et al. (2020) summarised and categorised previous indexes into four types: single-grading index, global-grading index, fines-content index, and grain-area index. The global-grading

index is more widely used, as the grain-area index has the disadvantage that it requires many assumptions, while the single-grading and fine-content indexes cannot represent the crushing of particles of different sizes (Xiao et al., 2020). The relative breakage B_r proposed by Hardin (1985) is one of the typical global-grading indexes (Figure 2), and B_r can easily quantify the amount of crushing simply by sieving. In sandy soils, it has been stated that there is a close relationship between B_r and stress (Vilhar et al., 2013). However, B_r is only a numeric index of the relative amount of crushing from the same initial grain size, which means that samples with different initial gradings cannot be compared, and the physical meaning of the value is not defined. Despite these issues, B_r is widely used in many studies due to its simplicity.

In this study, B_r which has many previous studies and is easy to compare with other soil material is discussed. The amount of particle crushing was quantified using B_r, and the crushability was discussed in comparison with previous studies. At the end of each test, the drainage valve was closed and the back and cell pressure slowly reduced before the sample was collected. The samples were then dried in a drying oven at 100 °C for 24 hours and sieve tests were conducted. For sieving, both before and after the test, the samples were manually sieved for 3 min according to the sieving test method for volcanic granular soils (Sato et al., 2024). This was to minimise the effect of particle crushing due to friction during the sieving process, which is said to be more pronounced in the case of pumice fall deposit. Figure 3 shows the actual measured changes in particle size distribution. It can be observed that crushing progresses in each test and the particle size distribution curve moves to the left compared to the original one. B_r was calculated for each test case to quantify the crushing that occurred during the test.

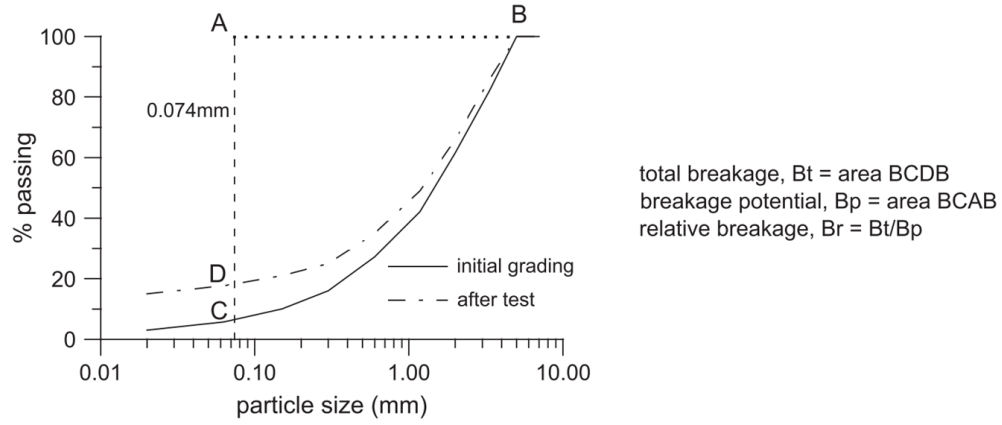

Figure 2. Definition of B_r redrawn by Vilhar et al. (2013) based on Hardin (1985).

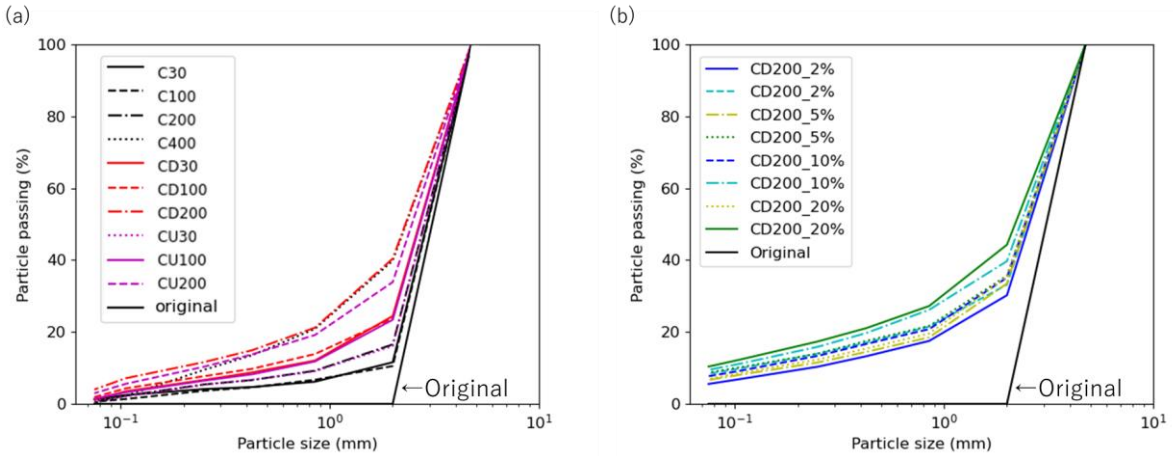

Figure 3. Particle size distribution curves of original and after each test of (a) ST series and (b) CE series.

3.3 Results of triaxial tests

Figure 4 shows the results of the standard triaxial series (ST series). In this study, figures including and following Figure 4 use specific markers to indicate test outcomes. Cases marked with a '★' at the test's end point are interpreted as not having reached the critical state. Conversely, cases denoted by a '×' signify that the critical state has been reached. In the CU tests, Ta-d pumice exhibited stress paths similar to those of very loose sand, and furthermore, when the axial strain exceeded about 5%, they reached critical state (steady state) where the axial strain progressed with constant deviator stress and effective mean stress. The mean effective stress moves in a decreasing direction after the onset of compression, and the position on the stress path of the phase transformation coincides with the critical state (steady state). This behaviour has a high potential for flow failure (Yoshimine and Ishihara, 1998). In the CD tests, Ta-d pumice showed a trend towards volumetric shrinkage and higher contraction in all cases. At confining pressure of 100 kPa and above in the CD test, the deviatoric stress and volumetric strain did not converge and continued to increase, and in some cases the critical state was not reached even at 20% axial strain.

Figure 5 presents the results of the crushing evolution series (CE series). Both CD and CU tests, similar to the standard triaxial series (ST series), exhibited highly compressible behaviour. For both types of tests, the results at final axial strains of 2%, 5%, and 10% closely overlapped with those at 20% axial strain, demonstrating the reproducibility of the experiments.

3.4 Relation of pressure to crushing

Figure 6 shows the $e - \log p'$ planes for the consolidation and compression processes of ST series, with the amount of crushing amount (B_r) at the end of each test on the graph. The $e - \log p'$ curves show that the endpoint of the compression test is not settled on a single line. The endpoints of the tests are located discretely, even taking into account that in two cases of the CD test the critical state is not reached. This can be attributed to the different position of the CSL on the $e - \log p'$, because each case has a different amount of crushing and can therefore be regarded as a different material with a different soil gradation.

Figure 7 shows B_r in each case plotted against p' at the end of the test in ST series. A relationship was observed where the amount of crushing increased with increasing pressure. Looking at Figure 7 it can be seen that for Ta-d pumice, the isotropic consolidation, CU and CD plots are represented by separate lines. This is due to the difference in void ratios at critical state, which will be discussed below. The plots with the values at the end of each test in ST series on the $e - p' - B_r$ space are shown in Figure 8 as the graphs are three-dimensional, they are illustrated from two angles. As it appears from Figure 8 that all the plots are almost on one plane, it is assumed that they can all be plotted on the same plane, and the plane ($e = -18.56B_r - 1.32\, log_{10}\, p' + 10.03$) that is most consistent with the experimental data is also shown using the least-squares method. This plane is referred to as “Crushing Surface” in a past study (Sato et al., 2024). Interestingly, the plots for the CD tests at confining pressures of 100 kPa and 200 kPa, which did not reach critical state, and for isotropic consolidation plots, are also located on this one plane. By using the three axes $e - p' - B_r$, the end states of CD and CU, which were represented as separate lines in Figure 7(b), can each be represented in one plane. The difference in the position of the critical states of CD and CU on the plane of p' and crushing amount in Figure 7 can be explained as being due to the difference in the void ratio. Thus, in pumice, not only the critical state, but also deformation progressing with particle crushing under certain conditions, such as isotropic consolidation, may always converge to a certain plane “Crushing Surface" on the $e - p' - B_r$ space.

Figure 9 shows the relationship between the amount of crushing and pressure in the CE series. The positions of the isotropic consolidation lines from the ST series (as shown in Figure 7) are also displayed in this figure. In the CD tests, it is observed that the amount of crushing increases with the progression of axial strain. However, in the CU tests, while an increase in crushing is seen up to 10% axial strain, there is hardly any difference in the amount of crushing between the 10% and 20% axial

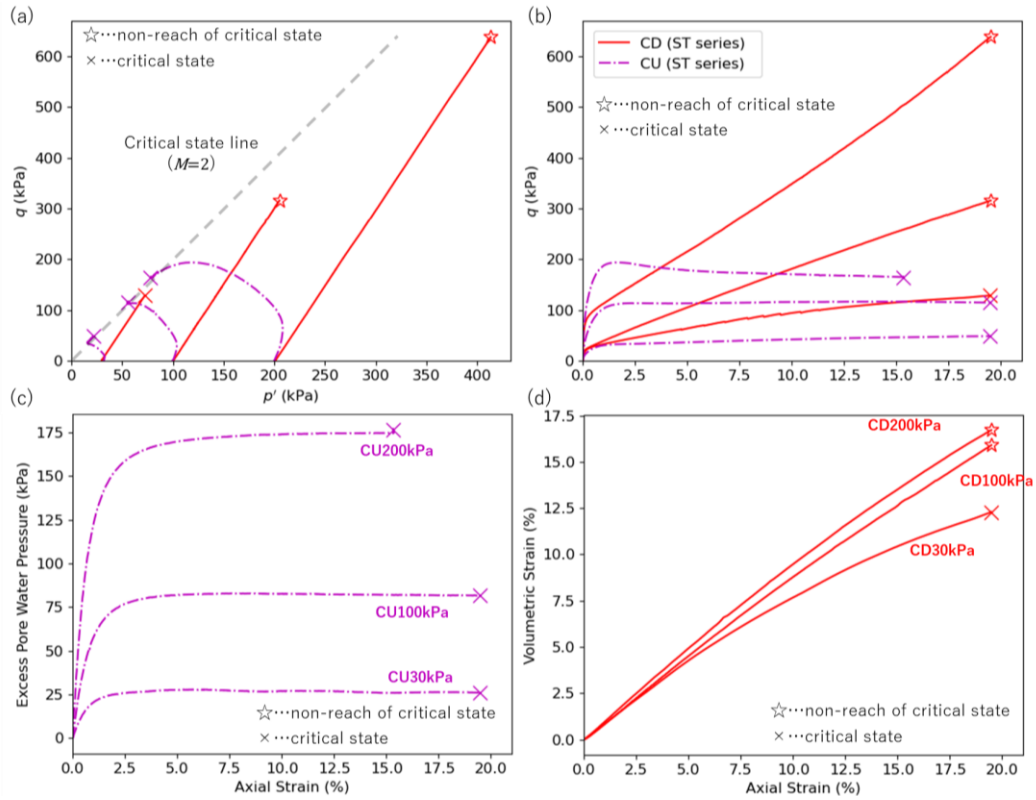

Figure 4. Triaxial compression test results of the ST series: (a) Effective stress paths, (b) deviator stress – axial strain relations, (c) excess pore water pressure – axial strain relations during undrained compression, and (d) volumetric strain – axial strain relations during drained compression.

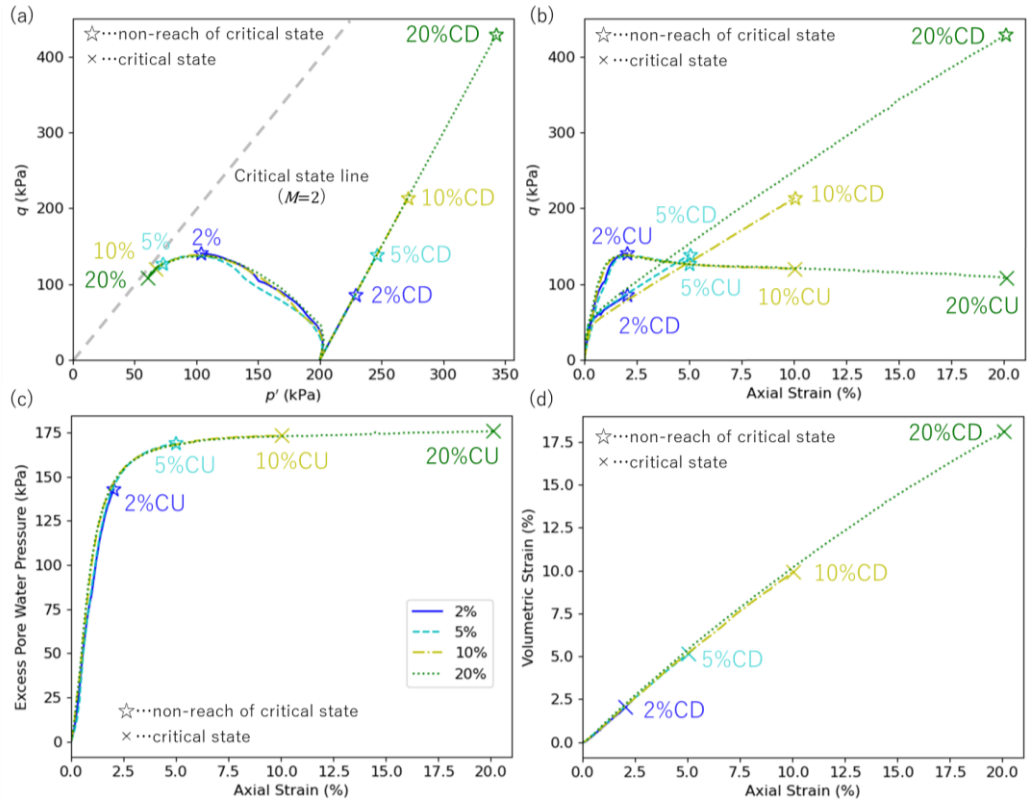

Figure 5. Triaxial compression test results of the CE series (at confining pressure of 200 kPa): (a) Effective stress paths, (b) deviator stress – axial strain relations, (c) excess pore water pressure – axial strain relations during undrained compression, and (d) volumetric strain – axial strain relations during drained compression.

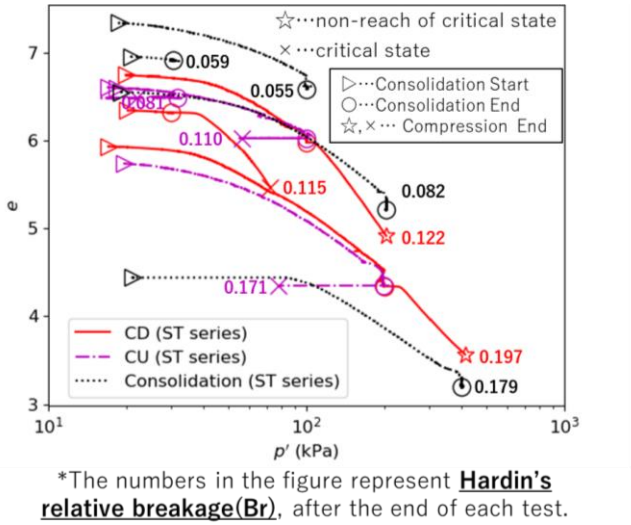

Figure 6. $e-\log p'$ curves for consolidation and compression processes of the ST series (after Fig. 15 of Sato et al., 2024a).

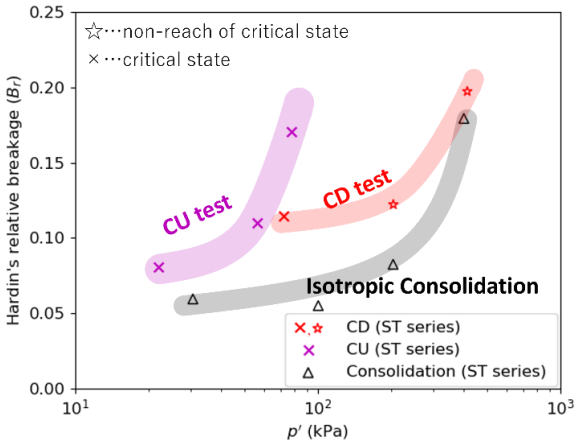

Figure 7. Relationship between Hardin's relative breakage (B_r) and effective mean principal stress at the end of the test in the ST series (after Fig. 16 of Sato et al., 2024a).

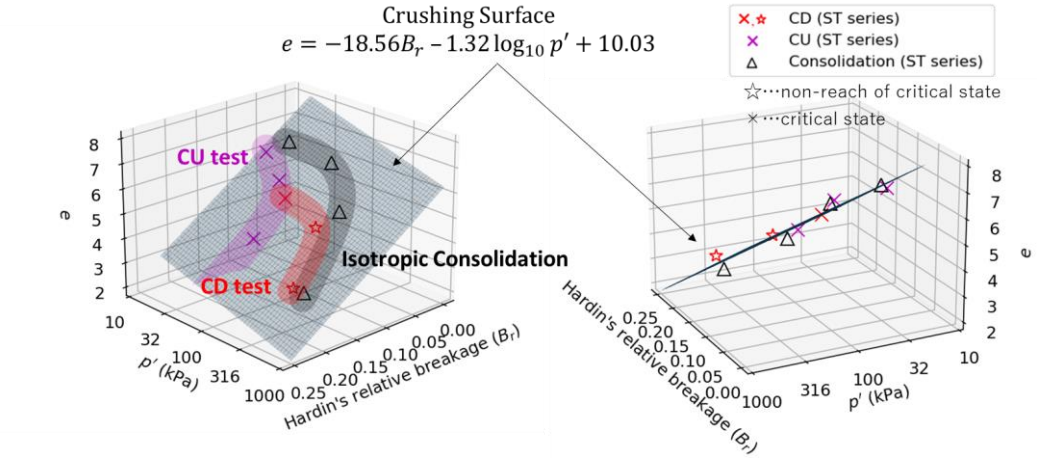

Figure 8. Crushing Surface of the ST series from two angles of view (after Fig. 18 of Sato et al., 2024a).

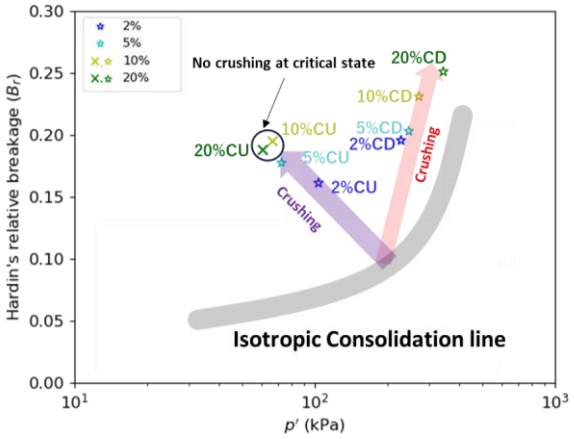

Figure 9. Relationship between Hardin's relative breakage (B_r) and effective mean principal stress at the end of the test in the CE series.

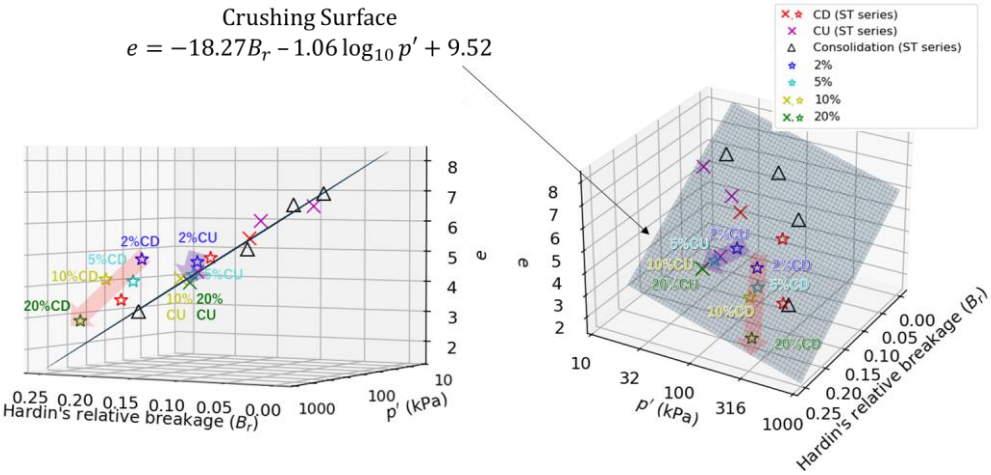

Figure 10. Crushing Surface of the CE and the ST series from two angles of view.

strain cases. This suggests that in crushed soils which have reached a critical state, crushing may not progress significantly.

The results of the CE series, plotted at the end of each test on the $e - p' - B_r$ space, are shown in Figure 10. Using the least squares method, the most consistent Crushing Surface ($e = -18.27B_r - 1.06\, log_{10}\, p' + 9.52$) was derived from the points that reached the critical state and isotropic consolidation (marked as '×' and 'triangle' in the figure). Figure 10 shows that in the CU tests, the plots at 2% axial strain did not reach the Crushing Surface, but by 5% strain, they were almost touching it, and by 10% and 20% strain, they were plotted at virtually the same position on the Crushing Surface. This indicates that in CU tests, the plots are positioned on the Crushing Surface after isotropic consolidation, and although they initially move away from this surface when compression loading begins, they return to the Crushing Surface upon reaching the critical state. On the other hand, the plots from the CD tests show that with increasing axial strain, the volume continues to contract while the pressure and amount of crushing increase, asymptotically approaching the Crushing Surface.

The above suggests that the mechanical behaviour of crushable porous particles may be described by organising them in the Crushing Surface (Sato et al., 2024a) on the space of void ratio, stress and amount of crushing. Thus, to understand the mechanical behaviour of pumice, it is important not only to focus on stress and crushing, but also to analyse changes in void ratio. In past studies on pumice, there has been little research measuring grain size changes after testing, and the relationship between the critical state line and crushing has remained unclear. Therefore, the Crushing Surface,

which can represent changes in the critical state line due to crushing of porous granular materials, is an innovative concept. The results of this study clarify how pumice approaches the critical state line, and these findings are expected to be useful in the future development of constitutive models for porous granular materials.

4 CONCLUSIONS

Isotropic consolidation, CD triaxial and CU triaxial tests were carried out on porous particles of Ta-d pumice, all starting from the same soil grading, to systematically investigate the relationship between particle crushing and the mechanical behaviour of crushable porous materials.

As a result, the following results and conclusions were obtained

- Crushable porous granular material has a high intra-particle void ratio, which correlates with particle size and is basically higher the larger the particles. Ta-d pumice, a natural pumice, has particularly high intra-particle voids.
- Crushable porous granular material is highly compressible and its stress path is similar to that obtained in undrained triaxial tests on very loose sand, leading to the critical state (steady state).
- The graphs of particle crushing versus effective mean stress at the end of the tests could be represented by a single curve for the isotropic consolidation test, CD and CU triaxial tests, respectively.
- The critical state of the crushable porous granular material can be represented by a single surface （Crushing Surface） in the space of three axes: particle crushing volume, voids ratio and mean effective stress at the end of the test. Furthermore, the isotropic consolidation state may also be plotted on the same surface.
- Crushable porous soil in the CD and CU tests increases the amount of crushing with increasing axial strain, moving toward the Crushing Surface in the three-dimensional space of stress, amount of crushing, and void ratio.
- Crushable porous soil in the CU tests shows that after reaching the critical state, the amount of crushing hardly increases even with further increases in axial strain.

The insights gained from this study, aimed at systematizing the crushing and mechanical behaviour of porous granular materials, are likely applicable to other porous granular bodies as well. If this research progresses further and the relationship between the critical state and crushing of porous granular materials is fully established, it may become possible to extend existing sand response models based on critical state theory to develop a constitutive model for crushable pumice. Once such a constitutive model is established, deformation analyses of pumice ground and simulations of large-scale flow events using analytical methods such as FEM or MPM will become feasible. Improved predictive accuracy of porous granular material ground behavior, which has previously required site-specific mechanical testing as "special soils," could enable practical applications such as slope flow risk assessments. However, the mechanics of porous granular materials remain insufficiently understood, and further fundamental research is necessary.

DISCLAIMER

The authors declare no conflict of interest.

AVAILABILITY OF DATA AND MATERIALS

All data are available from the author.

ACKNOWLEDGMENTS

This work was supported by JSPS KAKENHI Grant Number 19J20672.

REFERENCES

Altuhafi, F.N. & Coop, M.R., 2011. Changes to particle characteristics associated with the compression of sands. *Géotechnique*, 61(6), pp.459–471. https://doi.org/10.1680/geot.9.P.114

Bandini, V. & Coop, M.R., 2011. The Influence of Particle Breakage on the Location of the Critical State Line of Sands. *Soils and Foundations*, 51(4), pp.591–600. https://doi.org/10.3208/sandf.51.591

Been, K. & Jefferies, M.G., 1985. A state parameter for sands. *Géotechnique*, 35(2), pp.99–112. https://doi.org/10.1680/geot.1985.35.2.99

Castro, G., 1969. *Liquefaction of Sands*. Harvard University, Harvard Soil Mechanics Series 81.

Chiaro, G., Kiyota, T., Umar, M. & Cappellaro, C., 2022. Earthquake-Induced Flow-Type Slope Failure in Weathered Volcanic Deposits—A Case Study: The 16 April 2016 Takanodai Landslide, Japan. *Geosciences*, 12(11), p.394. https://doi.org/10.3390/geosciences12110394

de Cristofaro, M., Olivares, L., Orense, R.P., Asadi, M.S. & Netti, N., 2022. Liquefaction of Volcanic Soils: Undrained Behavior under Monotonic and Cyclic Loading. *Journal of Geotechnical and Geoenvironmental Engineering*, 148(1), pp.1–11. https://doi.org/10.1061/(ASCE)GT.1943-5606.0002715

Gajo, A., Muir Wood, D., 1999. Severn–Trent sand: a kinematic-hardening constitutive model: the q–p formulation. *Géotechnique*, 49(5), 595–614. https://doi.org/10.1680/geot.1999.49.5.595

Hardin, B.O., 1985. Crushing of Soil Particles. *Journal of Geotechnical Engineering*, 111(10), pp.1177–1192. https://doi.org/10.1061/(ASCE)0733-9410(1985)111:10(1177)

Hashimoto, H., Horinouchi, K., Sato, I. & Kuno, M., 2023. Soil Structure in Volcanic Pumice Soil of Dozou-sawa River Evaluated from In Situ and Laboratory Tests. *Geotechnical Testing Journal*, 46(6), p.20230324. https://doi.org/10.1520/GTJ20230324

Hyodo, M., Hyde, A.F.L. & Aramaki, N., 1998. Liquefaction of crushable soils. *Géotechnique*, 48(4), pp.527–543.

Ishihara, K., Tatsuoka, F. & Yasuda, S., 1975. Undrained Deformation and Liquefaction of Sand Under Cyclic Stresses. *Soils and Foundations*, 15(1), pp.29–44. https://doi.org/10.3208/sandf1972.15.29

Ishikawa, T., Miura, S., Uzuoka, R., Yasuda, S., Tatsuoka, F., Toyooka, Y., 2021. Reconnaissance report on geotechnical damage caused by 2018 Hokkaido Eastern Iburi earthquake with JMA seismic intensity 7. *Soils and Foundations*, 61(4), pp.1151–1171. https://doi.org/10.1016/j.sandf.2021.06.006

Ishikawa, T. & Miura, S., 2011. Influence of Freeze-Thaw Action on Deformation-Strength Characteristics and Particle Crushability of Volcanic Coarse-Grained Soils. *Soils and Foundations*, 51(5), pp.785–799. https://doi.org/10.3208/sandf.51.785

Kawamura, S., Takahashi, A., Sugiura, T., Nakamura, S., Yamada, S., 2019. Slope failures/landslides over a wide area in the 2018 Hokkaido Eastern Iburi earthquake. *Soils and Foundations*, 59(6), pp.2376–2395. https://doi.org/10.1016/j.sandf.2019.08.009

Li, R., Wang, F. & Zhang, S., 2020. Controlling role of Ta-d pumice on the coseismic landslides triggered by 2018 Hokkaido Eastern Iburi Earthquake. *Landslides*, 17(5), pp.1233–1250. https://doi.org/10.1007/s10346-020-01349-y

Sasitharan, S., Robertson, P.K., Sego, D.C. & Morgenstern, N.R., 1994. State-boundary surface for very loose sand and its practical implications. *Canadian Geotechnical Journal*, 31(3), pp.321–334. https://doi.org/10.1139/t94-040

Sato, I., Kuwano, R. & Otsubo, M., 2024. Particle crushing and critical state of volcanic pumice – 2018 Hokkaido Eastern Iburi Earthquake. *Soils and Foundations*, 64(3), p.101465. https://doi.org/10.1016/j.sandf.2024.101465

Sugimoto, H., Takeshi, T., Uto, T. & Honma, H., 2013. *Geomorphologic and Geologic Features of Landslides Induced by the 2011 Off the Pacific Coast of Tohoku Earthquake, in Shirakawa Hills, Fukushima Prefecture*. In: Earthquake-Induced Landslides, pp.189–201. https://doi.org/10.1007/978-3-642-32238-9_20

Vilhar, G., Jovičić, V. & Coop, M.R., 2013. The role of particle breakage in the mechanics of a non-plastic silty sand. *Soils and Foundations*, 53(1), pp.91–104. https://doi.org/10.1016/j.sandf.2012.12.006

Wesley, L.D., 2001. Determination of specific gravity and void ratio of pumice materials. *Geotechical Testing Journal*, 24, pp. 418-422. https://doi.org/10.1520/GTJ11139J

Xiao, Y., Desai, C.S., Daouadji, A., Stuedlein, A.W., Liu, H. & Abuel-Naga, H., 2020. Grain crushing in geoscience materials–Key issues on crushing response, measurement and modeling: Review and preface. *Geoscience Frontiers*, 11(2), pp. 363–374. https://doi.org/10.1016/j.gsf.2019.11.006

Yoshimine, M. & Ishihara, K., 1998. Flow Potential of Sand During Liquefaction. *Soils and Foundations*, 38(3), pp.189–198. https://doi.org/10.3208/sandf.38.3_189

Zhang, S., Wang, F., Li, R., Chen, Z., 2019. Characteristics of landslides triggered by the 2018 Hokkaido Eastern Iburi earthquake, Northern Japan. *Landslides*, 16(9), pp.1691–1708. https://doi.org/10.1007/s10346-019-01207-6

- This page is intentionally left blank -